Available online at www.eccomasproceedia.org
Eccomas Proceedia COMPDYN (2017) 1-19

ECCOMAS
Proceedia

COMPDYN 2017
6thECCOMAS Thematic Conference on
Computational Methods in Structural Dynamics and Earthquake Engineering
M. Papadrakakis, M. Fragiadakis (eds.)
Rhodes Island, Greece, 15–17June 2017

SECOND-ORDER TORSIONAL WARPING MODAL ANALYSIS OF THIN-WALLED BEAMS (COMPDYN 2017)

J. Murin[1], M. Aminbaghai[2], J. Hrabovsky[1], H. Mang[2,3]

[1] Faculty of Electrical Engineering and Information Technology
Slovak University of Technology, Ilkovičova 3, 812 19 Bratislava, Slovakia
justin.murin@stuba.sk, juraj.hrabovsky@stuba.sk

[2] Institute for Mechanics of Materials and Structures
Vienna University of Technology, Karlsplatz 3, A/1040 Vienna, Austria
mehdi.aminbaghai@tuwien.ac.at,herbert.mang@tuewien.ac.at

[3]National RPGE Chair Professor, Tongji University, Siping Road 1239, Shanghai, China,
herbert.mang@tuewien.ac.at

Keywords: Thin-walled Beams, Torsional Warping, Modal Analysis, Longitudinally Varying Axial Force.

Abstract. *This paper contains an investigation of the influence of the varying axial force and of Secondary Torsion Moment Deformation Effects (STMDE) on the deformations of thin-walled beams due to torsional warping. The investigation is based on second-order torsional warping theory of doubly symmetric thin-walled open and closed cross-sections. The axial force resulting from the torsional stiffness of the beams is considered by means of second-order torsional warping theory. The solutions of the underlying differential equations are used for setting up relations needed in the framework of the transfer matrix method. These relations permit consideration of both static and dynamic action. On the basis of these relations, the local finite element equations of twisted beams are established. The numerical investigation consists of modal analysis of thin-walled beams with open I and rectangular hollow cross-sections. The results are compared with finite element solutions obtained with standard solid and beam finite elements.*

© 2017 The Authors. Published by Eccomas Proceedia.
Peer-review under responsibility of the organizing committee of COMPDYN 2017.
doi: 10.7712/120117.5406.16926

1 INTRODUCTION

Recent research results have shown that for elastostatic non-uniform torsion of beams with closed cross-sections the influence of the Secondary Torsion-Moment Deformation-Effect (STMDE) is particularly significant. On the other hand, the influence of the STMDE by non-uniform elastostatic torsion of the open thin-walled sections is not significant. A broad comprehensive overview of the literature dealing with the issue of non-uniform torsion of thin-walled beams can be found, for example, in [1] and [2]. Thin-walled beam structures are frequently exposed to dynamic loads. Commercial FEM codes enable modal and transient analysis by 3D finite beam elements without and with consideration of warping [3]-[5]. For torsion, very often an improved Saint-Venant theory is used and special mass matrices are considered. In general, the bicurvature is chosen as an additional warping degree of freedom, and the STMDE is not considered (ref. [5] is an exception). The beam element in [4] can be used with a lumped or a consistent mass matrix. The consistent mass matrix includes warping effects, but does not include the effect of shear deformations. For standard beam elements, the consistent mass matrix is based on reference [6], with the exception of additional terms arising from the warping constant I_ω .For the warping element, lumped masses for the warping degree of freedom (bicurvature) are defined in [7]. As stated in [4], for solid and closed thin-walled sections, standard finite beam elements can be used without significant error. However, for open thin-walled sections, warping finite beam elements should be used. In [5], however, the warping finite beam element is recommended only for use for open thin-walled section beams. In [8], a boundary element method is developed for the non-uniform torsional vibration problem of doubly symmetric constant cross-sections, accounting for non-uniform warping and secondary torsional shear deformation-effects. Dynamic analysis of 3D beam elements, restrained at their edges and subjected to arbitrarily distributed dynamic loading is described in [9]. In [10], an elastic non-uniform torsion analysis of simply or multiply connected cylindrical bars with arbitrary cross-sections accounts for the effect of geometric non-linearity in the framework of the boundary-element method. In [11], the effect of rotary and warping inertia is considered. Nonlinear torsional vibrations of thin-walled beams, exhibiting primary and secondary warping, are investigated in [12]. A solution for the vibrations of Timoshenko beams by the isogeometric approach is presented in [13]. Warping effects, however, are not considered. In [14], geometrically non-linear free and forced vibrations of beams with non-symmetrical cross-sections are investigated by the Saint-Venant theory of torsion. Axial-torsional vibrations of rotating pretwisted thin-walled composite box beams, exhibiting primary and secondary warping, are investigated in [15]. A formulation of a 3D beam element for computation of transversal and warping eigenmodes is presented in [16]. In [17], a new 3D finite element for geometrically nonlinear analysis of beams, made of Functionally Graded Material (FGM) with transversally varying material properties, is presented. The warping displacements are accurately predicted. In [1], the influence of torsional warping of open and closed cross-sections of twisted beams, made of materials with constant material properties, on their eigenvibrations is investigated, considering the secondary deformations due to the angle of twist. Since the bicurvature cannot be used in the constraint equations, see. e.g. [4], it was logical to consider the part of the first derivative of the angle of twist, caused by the bimoment, as the warping degree of freedom [18] also for modal analysis. The results from modal analysis, concerning non-uniform and uniform torsion of beams with open cross-sections, have shown large differences of the eigenfrequencies. This has corroborated the well-known fact that warping must be taken into account also for modal analysis of beams with open cross-sections, subjected to torsion. It was also verified that the STMDE does not play a significant role in modal torsion analysis of beams with open cross-sections. On the other hand, the torsional eigenfrequencies,

obtained in case of consideration of STMDE, are very close to the ones obtained by 3D solid finite elements. In contrast to open cross-sections, the influence of warping (with or without STMDE) on the non-uniform torsional eigenfrequencies of beams with rectangular hollow cross-sections is not significant. The best agreement of results obtained by solid finite elements and by the method proposed in [1] (both for the Saint-Venant and the warping beam solutions) is obviously achieved for the first torsional eigenfrequency. For the higher modes, the difference between corresponding results increases especially for short beams. Some higher torsional eigenmodes, calculated by means of solid finite elements, contain deformations of the sidewalls of the beams. This effect cannot be considered in a straightforward manner by finite beam elements with restrained and unrestrained warping. As shown in [19], all eigenfrequencies calculated by solid finite elements agree very well with results obtained by experimental measurements. Other very recent aspects in the area of numerical solutions of non-uniform torsion are treated in [20]-[24]. Finally, in [2], a boundary element solution is developed for dynamic analysis, considering warping of beams with arbitrary cross-sections, including shear lag effects due to both flexure and torsion. High accuracy of the results in comparison to the ones obtained by solid finite element solution is obtained. However, in the solid model, the distortion effect of the cross-section was restrained. A common feature of the above cited articles is disregard of the effect of the variable axial force on torsional warping.
In this paper, the work reported in [1] is extended to uniform and non-uniform torsional analysis of beams with a variable axial force. The differential equations of beams with such an axial force are formulated for Saint-Venant and non-uniform torsional deformations, including inertial line moments. In non-uniform torsion, the part of the bicurvature, caused by the bimoment, is taken into account as the warping degree of freedom, and the STMDE is also considered. A general semi-analytical solution of the differential equation is presented and the transfer matrix relation is established, from which the finite element equations for beam elements with two nodes are derived. Omitting the external load, the FEM equation for the torsional natural free vibrations is obtained. The numerical investigation deals with torsional modal analysis of thin-walled beams with I cross-sections and rectangular hollow cross-sections. The obtained results are compared with the ones from commercial FEM codes. The effect of the axial force is evaluated.

2 EQUATIONS OF NONUNIFORM TORSION WITH EFECT OF STMDE AND VARIABLE AXIAL FORCE

According to the theory of second-order torsional warping, the axial forces affect the torsional stiffness GI_T, where G is the shear modulus and I_T is the torsion constant. Basically, compression results in a decrease and traction in an increase of the torsional stiffness GI_T of the beam. This situation may be considered by an additional stiffness $N i_p^2$ (e.g. [25]) for doubly symmetric cross-sections, where N is the known axial force, acting at the center point of the cross-section, and $i_p = \sqrt{I_P / A}$ denotes the radius of gyration and I_P is the polar moment of area. In case of a variable axial force $N^{II}(x) = N(x)$, the corresponding variable torsional stiffness is obtained as $GI_T^*(x) = GI_T + N^{II}(x) i_p^2$, where the term $N^{II}(x) i_p^2$ denotes the so-called geometric stiffness. Representing a load, the axial force $N(x)$ appears in the respective term of the differential equation for the displacement in the longitudinal direction. The variable axial force $N^{II}(x)$ appears in the homogeneous part of the differential equation for the angle

of twist. The variation of the known axial force $N^{II}(x)$ accounts for the stiffening or softening of the torsional stiffness in the framework of the second-order torsional warping theory. For doubly symmetric cross-sections, the torsional deformations are decoupled from the bending deformations and the longitudinal deformations. For this case, the differential equation for the angle of twist will be presented in this Chapter.

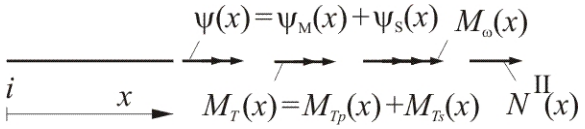

Figure 1: Second-order torsional warping theory: axial force, torsional moments and angles of twist.

Figure 1 refers to the second-order torsional warping theory. It shows the axial force $N^{II}(x)$, the torsional moment $M_T(x)$ as the sum of the primary torsional moment, $M_{Tp}(x)$, and the secondary torsional moment, $M_{Ts}(x)$, and the bimoment $M_\omega(x)$. Figure 1 also shows the angle of twist, $\psi(x)$, corresponding to $M_{Tp}(x)$. It represents the sum of the angle of twist, resulting from the primary deformation, $\psi'_M(x)$, and the secondary deformation $\psi'_S(x)$.

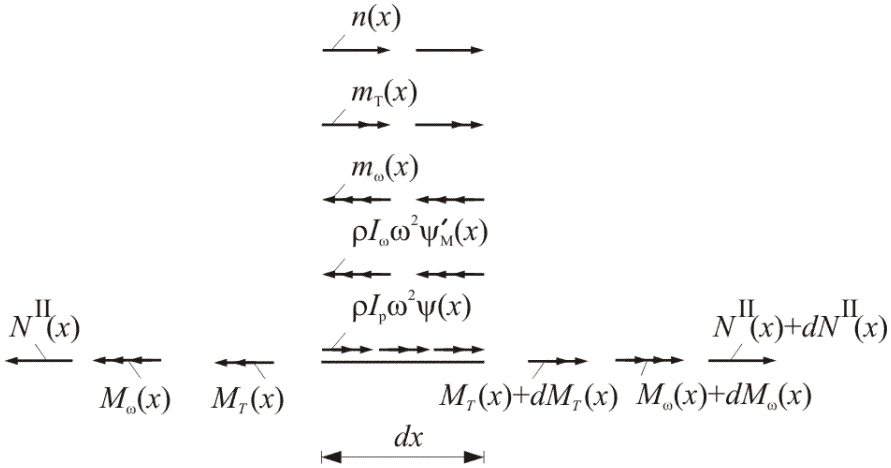

Figure 2: Second-order torsional warping theory: static load and moments and static equivalent of the respective dynamic load, acting on an infinitesimal beam element.

Figure 2 illustrates an infinitesimal element of the beam. It is loaded by the torsional line moment $\rho I_p \omega^2 \psi(x)$ and the line bimoment $\rho I_\omega \omega^2 \psi'_M(x)$, where I_ω stands for the warping constant. These loads represent the static equivalent of the respective dynamic action. The static loads are the warping moment per unit length, m_ω, the torsional moment per unit length, m_T and the axial force per unit length, n. After some mathematical manipulation, a linear differential equation of 4th order for angle of twist according the second-order warping theory is obtained (its derivation is detailed given in our article [34]):

$$
\begin{aligned}
&EI_\omega\left(1+\frac{GI_T^*}{GI_{Ts}}\right)\psi''''(x)+3\frac{EI_\omega}{GI_{Ts}}GI_T^{*\prime}\psi'''(x)\\
&+\left(\frac{EI_\omega}{GI_{Ts}}\rho I_p\omega^2+3\frac{EI_\omega}{GI_{Ts}}GI_T^{*\prime\prime}+\rho I_\omega\omega^2+GI_T^*\left(\frac{\rho I_\omega\omega^2}{GI_{Ts}}-1\right)\right)\psi''(x)\\
&+\left(\frac{EI_\omega}{GI_{Ts}}GI_T^{*\prime\prime\prime}+GI_T^{*\prime}\left(\frac{\rho I_\omega\omega^2}{GI_{Ts}}-1\right)\right)\psi'(x)+\rho I_p\omega^2\left(\frac{\rho I_\omega\omega^2}{GI_{Ts}}-1\right)\psi(x)\\
&=-\left(\frac{\rho I_\omega\omega^2}{GI_{Ts}}-1\right)m_T(x)-\frac{EI_\omega}{GI_{Ts}}m_T''(x)-m_\omega'(x).
\end{aligned}
\qquad (1)
$$

The above differential equation, with variable coefficients $\left(\eta_k(x), k\in\langle 0,4\rangle\right)$, can formally be written as

$$\eta_4(x)\psi''''(x)+\eta_3(x)\psi'''(x)+\eta_2(x)\psi''(x)+\eta_1(x)\psi'(x)+\eta_0(x)\psi(x)=\eta_L(x), \qquad (2)$$

where $\eta_L(x)$ is the polynomial distributed load [34]. In case of a constant torsional stiffness ($N^{II}(x)=0\Rightarrow GI_T^*=GI_T$), equation (1) belongs to the category of non-uniform torsion (first-order torsional warping theory, e.g. [1]). Equation (1) represents the mathematical formulation of the second-order torsional warping theory with consideration of the secondary torsion-moment deformation-effect (e.g. [25]).

Neglecting this effect by setting $GI_{Ts}=\infty$, and setting $I_\omega=0$, equation (1) degenerates to the respective relation in the framework of Saint-Venant torsion, including the effect of the variable axial force, which results in the geometric stiffness. Thus,

$$GI_T^*\psi''(x)+GI_T^{*\prime}\psi'(x)+\rho I_p\omega^2\psi(x)=-m_T(x). \qquad (3)$$

The general semi-analytical solution of the differential equation (2) can be found as follows [27]:

$$\psi(x)=b_0(x)\psi_i+b_1(x)\psi_i'+b_2(x)\psi_i''+b_3(x)\psi_i'''+\sum_{s=0}^{\max s}\eta_{L,s}b_{s+4}(x), \qquad (4)$$

where $b_0(x)$, $b_1(x)$, $b_2(x)$, $b_3(x)$,…, $b_{s+4}(x)$, $s\in<0, max\ s>$, denote the transfer functions [27] and ψ_i, ψ_i', ψ_i'', ψ_i''' represent the integration constants, referring to the starting point *i*. After some mathematical manipulations, the solution of (4) can be found:

$$\underbrace{\left|\begin{array}{c}\psi(x)\\ \psi'(x)\\ \psi''(x)\\ \psi'''(x)\\ \hline 1\end{array}\right|}_{\boldsymbol{\psi}(x)} = \underbrace{\left|\begin{array}{cccc|c} b_0(x) & b_1(x) & b_2(x) & b_3(x) & \sum_{s=0}^{\max s}\eta_{Ls}b_{s+4}(x)\\ b_0'(x) & b_1'(x) & b_2'(x) & b_3'(x) & \sum_{s=0}^{\max s}\eta_{Ls}b_{s+4}'(x)\\ b_0''(x) & b_1''(x) & b_2''(x) & b_3''(x) & \sum_{s=0}^{\max s}\eta_{Ls}b_{s+4}''(x)\\ b_0'''(x) & b_1'''(x) & b_2'''(x) & b_3'''(x) & \sum_{s=0}^{\max s}\eta_{Ls}b_{s+4}'''(x)\\ \hline 0 & 0 & 0 & 0 & 1\end{array}\right|}_{\boldsymbol{B}(x)} \cdot \underbrace{\left|\begin{array}{c}\psi_i\\ \psi_i'\\ \psi_i''\\ \psi_i'''\\ \hline 1\end{array}\right|}_{\boldsymbol{\psi}_i} \tag{5}$$

In equation (5), $\boldsymbol{B}(x)$ is a matrix, containing the solution functions of the homogeneous differential equation and particular solution functions of the inhomogeneous part of the differential equation and their first three derivatives at x. $\boldsymbol{\psi}(x)$ is a vector, containing the angle of twist and its first three derivatives at x, and $\boldsymbol{\psi}_i$ is a vector, obtained by specialization of $\boldsymbol{\psi}(x)$ and its first three derivatives for the starting point i. The solution functions are calculated numerically by means of the algorithm published in [27].

In addition, by the approach described in [34], the transfer matrix method relation

$$\underbrace{\left|\begin{array}{c}\psi(x)\\ \psi'_M(x)\\ M_\omega(x)\\ M_T(x)\\ \hline 1\end{array}\right|}_{\boldsymbol{Z}(x)} = \underbrace{\left|\begin{array}{cccc|c} f_{11} & f_{12} & f_{13} & f_{14} & f_{15}\\ f_{21} & f_{22} & f_{23} & f_{24} & f_{25}\\ f_{31} & f_{32} & f_{33} & f_{34} & f_{35}\\ f_{41} & f_{42} & f_{43} & f_{44} & f_{45}\\ \hline 0 & 0 & 0 & 0 & 1\end{array}\right|}_{\boldsymbol{F}_{xi}(x)} \cdot \underbrace{\left|\begin{array}{c}\psi_i|_{x=0}\\ \psi'_{M,i}|_{x=0}\\ M_{\omega,i}|_{x=0}\\ M_{T,i}|_{x=0}\\ \hline 1\end{array}\right|}_{\boldsymbol{Z}_i} \tag{6}$$

is obtained, where $\boldsymbol{Z}(x)$ is the "static vector", $\boldsymbol{Z}_i$ is the static vector at the starting point i and $\boldsymbol{F}_{xi}(x)$ is the transfer matrix [34].

By neglecting the secondary torsion-moment deformation-effect and setting the warping constant equal to zero, equation (6) degenerates to the relation for Saint-Venant torsion, including the influence of the variable axial force, resulting in a geometric stiffness. This gives

$$\underbrace{\left|\begin{array}{c}\psi(x)\\ M_T(x)\\ \hline 1\end{array}\right|}_{\boldsymbol{Z}(x)} = \underbrace{\left|\begin{array}{ccc} b_0(x) & \dfrac{b_1(x)}{GI_{T,i}^*|_{x=0}} & \sum_{s=0}^{\max s}\eta_{Ls}b_{s+4}(x)\\ b_0(x)GI_T^* & \dfrac{b_1(x)GI_T^*(x)}{GI_{T,i}^*|_{x=0}} & GI_T^*(x)\sum_{s=0}^{\max s}\eta_{Ls}b_{s+4}'(x)\\ \hline 0 & 0 & 1\end{array}\right|}_{\boldsymbol{F}_{xi}(x)} \cdot \underbrace{\left|\begin{array}{c}\psi_i|_{x=0}\\ M_{T,i}|_{x=0}\\ \hline 1\end{array}\right|}_{\boldsymbol{Z}_i}. \tag{7}$$

3 FINITE BEAM ELEMENT EQUATION OBTAINED FROM THE TRANSFER MATRIX METHOD RELATION

Figure 3 illustrates the beam element. It is loaded by the inertial torsional line moment $\rho(x)I_p\omega^2\psi(x)$ and the inertial line bimoment $\rho(x)I_\omega\omega^2\psi'_M(x)$, the torsional line moment $m_T(x)$ and the torsional warping line moment $m_\omega(x)$ per unit length, where I_ω stands for the warping constant. These line moments represent the static equivalent of the respective dynamic action.

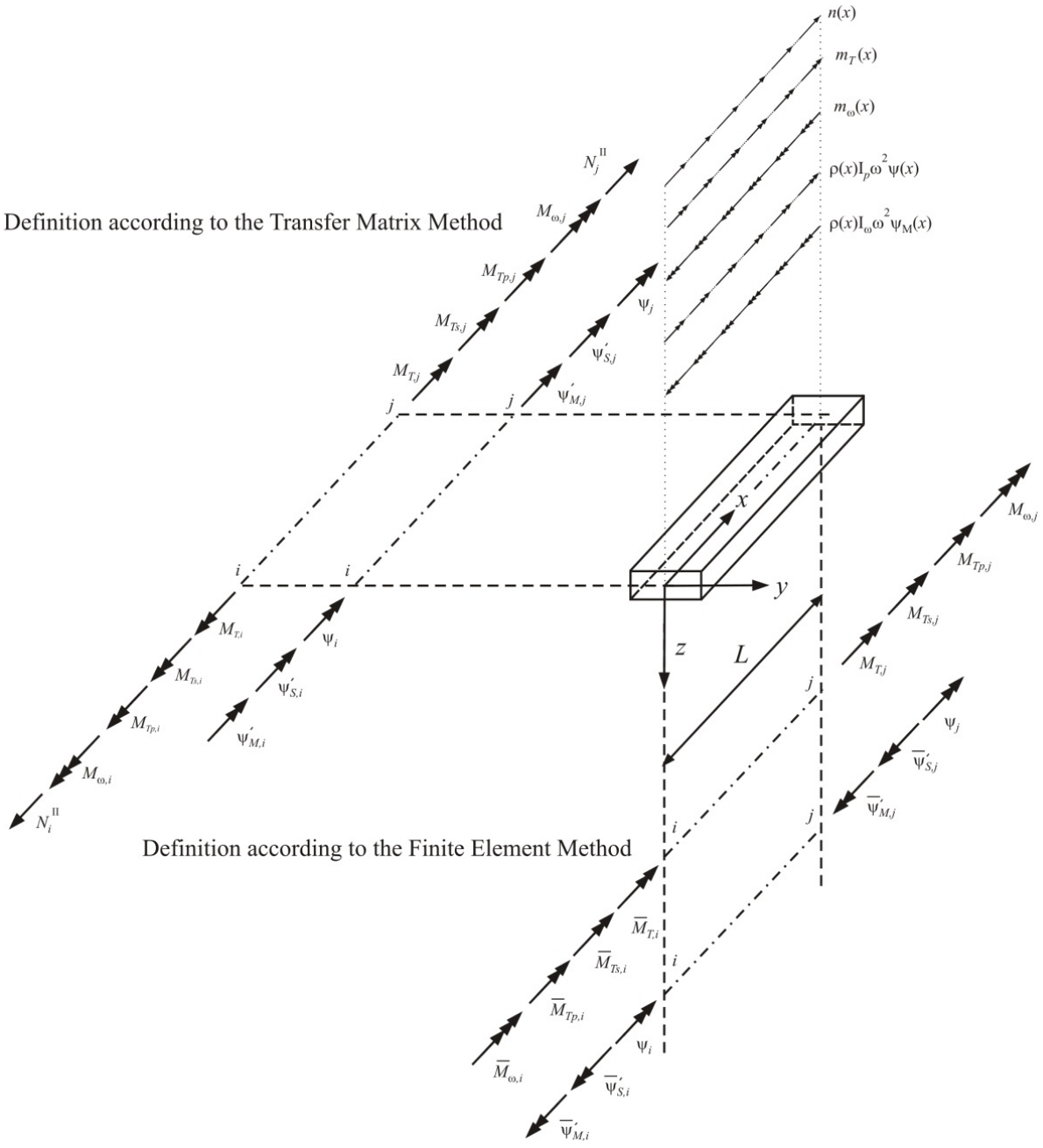

Figure 3: Positive orientation of the axial force, the torsional moments, and the rotation angles at the element nodes for the transfer matrix method and the finite element method.

The kinematic and kinetic variables at node *i* are denoted by the index *i* in (6) and in Figure 3. By setting $x = L$ in (6), the dependence of the nodal variables at node *j* on the nodal variables at node *i* is obtained. Then, using appropriate mathematical operations, the local finite element equations for the second-order torsional warping theory read as follows (considering the definition of a positive coordinate system in the framework of the finite element method, resulting in $\bar{M}_{T,i} = -M_{T,i}$, $\bar{M}_{\omega,i} = -M_{\omega,i}$, $\bar{\psi}'_{M,i} = -\psi'_{M,i}$ and $\bar{\psi}'_{M,j} = -\psi'_{M,j}$):

$$\begin{vmatrix} \bar{M}_{T,i} \\ \bar{M}_{\omega,i} \\ M_{T,j} \\ M_{\omega,j} \end{vmatrix} = \begin{vmatrix} K_{1,1} & K_{1,2} & K_{1,3} & K_{1,4} \\ K_{2,1} & K_{2,2} & K_{2,3} & K_{2,4} \\ K_{3,1} & K_{3,2} & K_{3,3} & K_{3,4} \\ K_{4,1} & K_{4,2} & K_{4,3} & K_{4,4} \end{vmatrix} . \begin{vmatrix} \psi_i \\ \bar{\psi}'_{M,i} \\ \psi_j \\ \bar{\psi}'_{M,j} \end{vmatrix} + \begin{vmatrix} K_{1,5} \\ K_{2,5} \\ K_{3,5} \\ K_{4,5} \end{vmatrix} . \tag{8}$$

The local finite element matrix $\boldsymbol{K}$ in (8) contains the linear and the geometric stiffness matrix and the consistent mass matrix.

By neglecting the secondary torsion-moment deformation-effect and by the setting warping constant equal to zero, equation (8) degenerates to the relations for Saint-Venant torsion, including the influence of the variable axial force, resulting in a geometric stiffness. This gives

$$\begin{vmatrix} \bar{M}_{T,i} \\ M_{T,j} \end{vmatrix} = \begin{vmatrix} \dfrac{b_0(x)\, GI^*_{T,i}\big|_{x=0}}{b_1(x)} & \dfrac{-GI^*_{T,i}\big|_{x=0}}{b_1(x)} \\ b_0(x) GI^*_T - \dfrac{b_1'(x) b_0(x) GI^*_T(x)}{b_1(x)} & \dfrac{b_1'(x) GI^*_T(x)}{b_1(x)} \end{vmatrix} . \begin{vmatrix} \psi_i \\ \psi_j \end{vmatrix} + \begin{vmatrix} \dfrac{GI^*_{T,i}\big|_{x=0} \sum\limits_{s=0}^{\max s} \eta_{Ls} b_{s+4}(x)}{b_1(x)} \\ GI^*_T(x) \left(\sum\limits_{s=0}^{\max s} \eta_{Ls} b'_{s+4}(x) - \dfrac{b_1'(x) \sum\limits_{s=0}^{\max s} \eta_{Ls} b_{s+4}(x)}{b_1(x)} \right) \end{vmatrix} . \tag{9}$$

4 NUMERICAL INVESTIGATION

The finite element relations were implemented into the software MATHEMATICA [28]. The numerical investigation includes torsional modal analyses of thin-walled beams under usual boundary conditions. Results of elastostatic analysis are presented in [34].

4.1 Torsional modal analyses of a beam with I cross-section, subjected to an axial load

The length of the beam, *L*, is 1.0, 1.5, 2.0, 2.5 and 3.0 m. The cross-section is the one of a HEB-500 [29]. In Table 1 and Table 2, the material properties and the cross-sectional parameters, respectively, are listed. The cantilever and clamped beam is considered. The Saint-Venant torsional and warping eigenfrequencies, and the radius of gyration, are calculated for the beam for a variable axial force $N^{II}(x)$, given as follows:

$$N^{\mathrm{II}}(x) = n_x(L - x) \quad , \forall n_x \in [-3000, 3000], \ \mathrm{kN/m} \tag{10}$$

The calculation of the eigenfrequencies according to the second-order torsional warping theory with STMDE consists of the following steps: At first, the transfer matrix $\boldsymbol{F}_{xi}(x)$, see equation (6), is specialized for L and for the nodes a and b (see Figure 4).

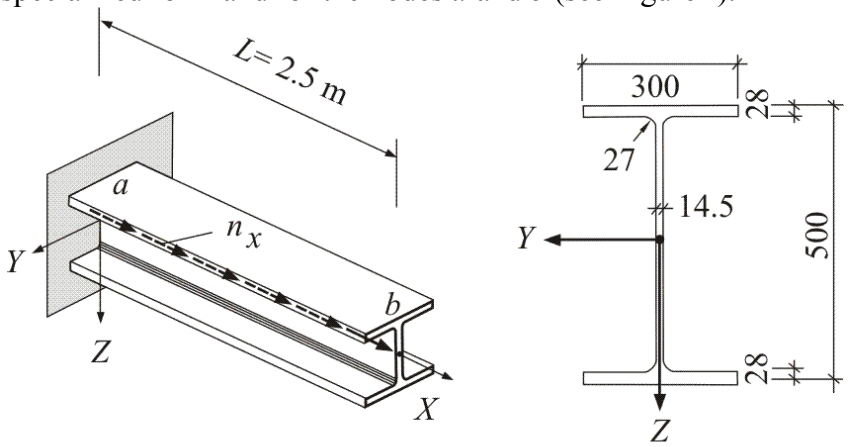

Figure 4: Cantilever beam with an I cross-section: a) system, axial line load, b) cross-section.

For modal analysis the influence of the load vector in the transfer matrix $\boldsymbol{F}_{ba}(x = L)$ is equal to zero. Taking the boundary conditions, given in equation (11), into account, the reduced system of two homogeneous algebraic equations is obtained. They represent an eigenvalue problem. The circular natural frequencies ω_{j}, $\mathrm{j} = 1, 2, \ldots$, follow from the zeros of the determinant of the reduced system of equations. An iterative method was used to find these zeros [1]. The natural frequencies $\mathrm{f}_{\mathrm{j}} = \omega_{\mathrm{j}} / 2\pi$, $\mathrm{j} = 1, 2, \ldots,$ are computed subsequently. In the same way, the calculation of the eigenfrequencies according to Saint-Venant torsion, including the influence of the variable axial-force effect is carried out.
The above algorithm was implemented into the software MATHEMATICA [28]. In this Subchapter, the results of the numerical experiments are presented and compared with the ones obtained by means of the available commercial software.

Material properties		
Young's modulus	$E = 21 \cdot 10^7$	kN/m²
Poisson's ratio	$\nu = 0.3$	
Shear modulus	$G = 8.0769 \cdot 10^7$	kN/m²
Mass density	$\rho = 7.85$	t/m³

Table 1: Material properties.

Cross-sectional parameters [29]		
Cross-sectional area	$A = 239 \cdot 10^{-4}$	m²
Shear area in the y - direction	$A_y = 140.27 \cdot 10^{-4}$	m²
Shear area in the z - direction	$A_z = 65.77 \cdot 10^{-4}$	m²
Second moment of area about the y-axis	$I_y = 107200 \cdot 10^{-8}$	m⁴

Second moment of area about the z-axis	$I_z = 12620 \cdot 10^{-8}$	m^4
Polar moment of area	$I_p = I_y + I_z = 119820 \cdot 10^{-8}$	m^4
Radius of gyration	$i_p = 22.41 \cdot 10^{-2}$	m
Torsion constant	$I_T = 538.4 \cdot 10^{-8}$	m^4
Secondary torsion constant	$I_{Ts} = 77974.4 \cdot 10^{-8}$	m^4
Warping constant	$I_\omega = 7017700 \cdot 10^{-12}$	m^6

Table 2: Cross-sectional parameters [29].

The following boundary conditions for cantilever beam (Figure 4) are applied:

a) Saint-Venant torsional vibrations:

$$\psi(x)\big|_{x=0} = \psi_a = 0, \; M_T(x)\big|_{x=L} = M_{T,b} = 0. \tag{11}$$

b) Warping vibrations:

$$\psi(x)\big|_{x=0} = \psi_a = 0, \qquad \psi'_M(x)\big|_{x=0} = \psi'_{M,a} = 0,$$
$$M_\omega(x)\big|_{x=L} = M_{\omega,b} = 0, \qquad M_T(x)\big|_{x=L} = M_{T,b} = 0. \tag{12}$$

Table 3 contains a comparison of the results for the first three torsional eigenfrequencies, obtained by the proposed method (Saint-Venant torsion and second-order torsional warping theory with STMDE), with corresponding results, obtained by the computer programs ANSYS [3], RSTAB [30], and RFEM [33] for the beam length L = 2.5 m. The computational models for the proposed method (Saint-Venant and warping torsion) consisted of only one finite beam element. Alternatively, 100 beam elements of RSTAB [30] were used for Saint-Venant modal analysis. This element does not allow consideration of a variable axial force. A very fine mesh, consisting of 16 080 3D-SOLID186 finite elements was used in the analysis by ANSYS [3], and 100 2D and 3D-Solid elements were used in the analysis RFEM [33]. The variation of the axial force in the 3D and 2D-Solid model was considered by applying mechanically consistent forces to the nodes of the elements.

eigenfrequencies for a variable axial force $N^{II}(x) = n_x(L-x)$ $\forall n_x \in [-3000, 3000]\left[\frac{\text{kN}}{\text{m}}\right]$			Proposed method	RSTAB [30] 100 beam-elements	RFEM [33] 100 2-D-Solid elements	RFEM [33] 100 3-D-Solid elements	ANSYS [3] 16080 SOLID186 elements
n_x = -3 000	Saint-Venant torsion	f_1	11.92	21.50	-------	-------	-------
		f_2	43.16	64.51	-------	-------	-------
		f_3	72.88	107.54	-------	-------	-------
	Warping torsion	f_1	42.35	-------	39.32	41.02	41.39
		f_2	217.03	-------	215.99	213.67	213.24
		f_3	543.14	-------	549.22	552.14	550.76

n_x= -2 000	Saint-Venant torsion	f_1	16.23	21.50	-------	-------	-------
		f_2	52.74	64.51	-------	-------	-------
		f_3	88.41	107.54	-------	-------	-------
	Warping torsion	f_1	43.33	-------	40.37	41.97	42.02
		f_2	218.08	-------	215.96	214.56	213.86
		f_3	544.33	-------	550.39	553.23	551.55
n_x= -1 000	Saint-Venant torsion	f_1	19.14	21.50	-------	-------	-------
		f_2	59.24	64.51	-------	-------	-------
		f_3	98.96	107.54	-------	-------	-------
	Warping torsion	f_1	44.28	-------	41.38	42.90	42.63
		f_2	219.12	-------	217.93	215.56	214.49
		f_3	545.52	-------	551.56	554.32	552.34
n_x= 0	Saint-Venant torsion	f_1	21.50	21.50	-------	-------	-------
		f_2	64.51	64.51	-------	-------	-------
		f_3	107.51	107.54	-------	-------	-------
	Warping torsion	f_1	45.21	-------	42.37	43.81	43.26
		f_2	220.16	-------	218.89	216.56	215.24
		f_3	546.70	-------	552.78	555.81	553.49
n_x= 1 000	Saint-Venant torsion	f_1	23.55	21.50	-------	-------	-------
		f_2	69.07	64.51	-------	-------	-------
		f_3	114.90	107.54	-------	-------	-------
	Warping torsion	f_1	46.12	-------	43.34	44.69	43.83
		f_2	221.19	-------	217.53	219.87	215.72
		f_3	547.88	-------	553.89	556.49	553.91
n_x= 2000	Saint-Venant torsion	f_1	25.38	21.50	-------	-------	-------
		f_2	73.16	64.51	-------	-------	-------
		f_3	121.51	107.54	-------	-------	-------
	Warping torsion	f_1	47.02	-------	44.28	45.56	44.42
		f_2	222.22	-------	218.51	220.84	216.33
		f_3	549.05	-------	555.05	557.58	554.70
n_x= 3 000	Saint-Venant torsion	f_1	27.06	21.50	-------	-------	-------
		f_2	76.89	64.51	-------	-------	-------
		f_3	127.54	107.54	-------	-------	-------
	Warping torsion	f_1	47.89	-------	45.21	46.41	44.96
		f_2	223.24	-------	219.48	221.81	216.93
		f_3	550.22	-------	556.21	558.66	555.48

Table 3: Comparison of the results for the eigenfrequencies obtained by the proposed method, [30], [33], with corresponding results, obtained by [3] for a cantilever beam with an I cross-section and a variable axial force.

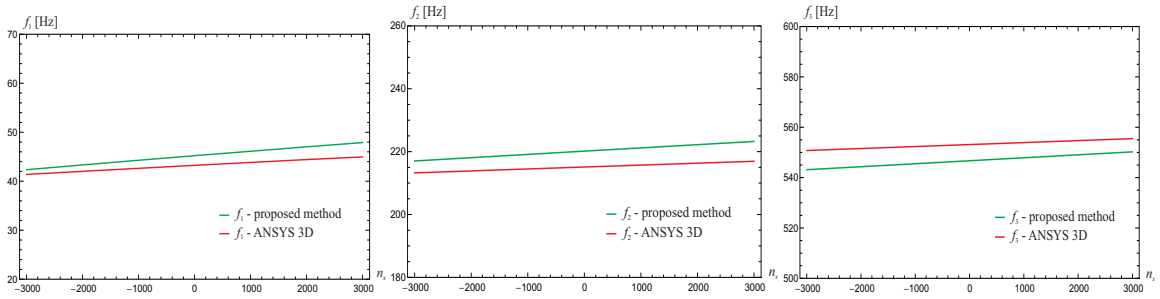

Figure 5: Comparison of the cantilever beam eigenfrequencies for $L = 2.5$ m.

As shown in Table 3 and Figure 5, the eigenfrequencies obtained by the proposed second-order torsional warping elements agree very well with the ones obtained with 3D-Solid elements. As expected, the Saint Venant solution (with and without the axial force effect) gave incorrect results. Analogous to the situation for bending vibrations, axial tension in addition to torsion results in an increase and axial compression in addition to torsion in a decrease of the torsional eigenfrequencies.

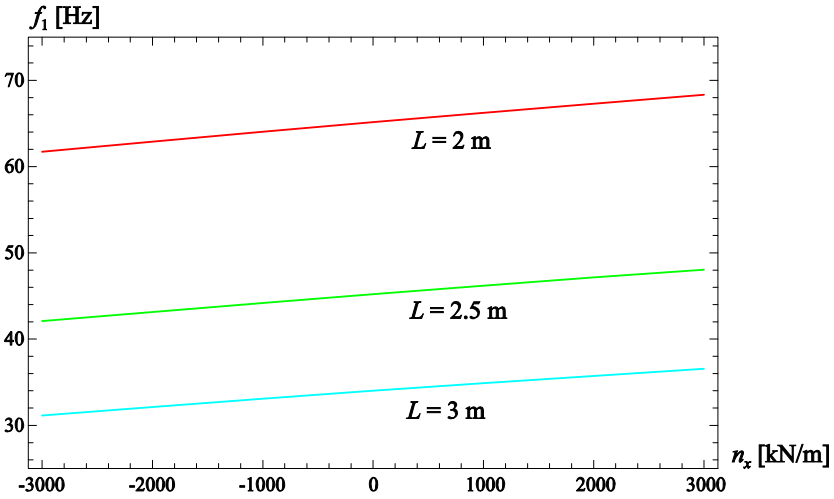

Figure 6: Dependence of the 1st eigenfrequency on the beam length for the cantilever beam that is calculated by the proposed method.

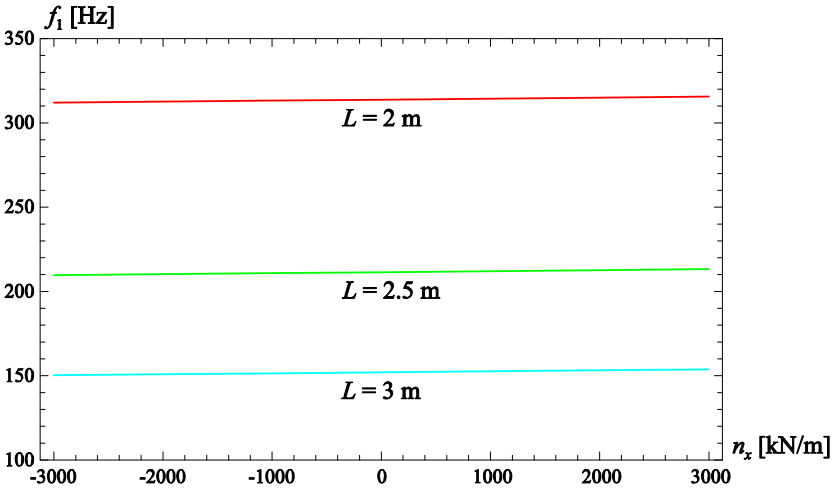

Figure 7: Dependence of the 1st eigenfrequency on the beam length for the clamped beam that is calculated by the proposed method.

In Figure 6 and 7, the 1st eigenfrequecy is shown for considered supports, beam lengths and the varying axial force, calculated by the proposed method. As expected, an increase of the beam length decreases the torsional warping eigenfrequencies. The greatest impact of the varying axial force on the eigenfrequency is by the cantilever beam. Similar results are also obtained for natural frequencies of higher order.

4.2 Torsional modal analyses of a cantilever beam with rectangular hollow cross-section, subjected to an axial load

The length of the beam, L, is 2.5 m. The material properties and the cross-sectional parameters are listed in Table 1 and Table 4, respectively. The modal analyses are performed for the beam for the following axial force: $N^{\mathrm{II}}(x) = n_x(L-x)$ for $n_x = 0$ and ±1000 kN/m.

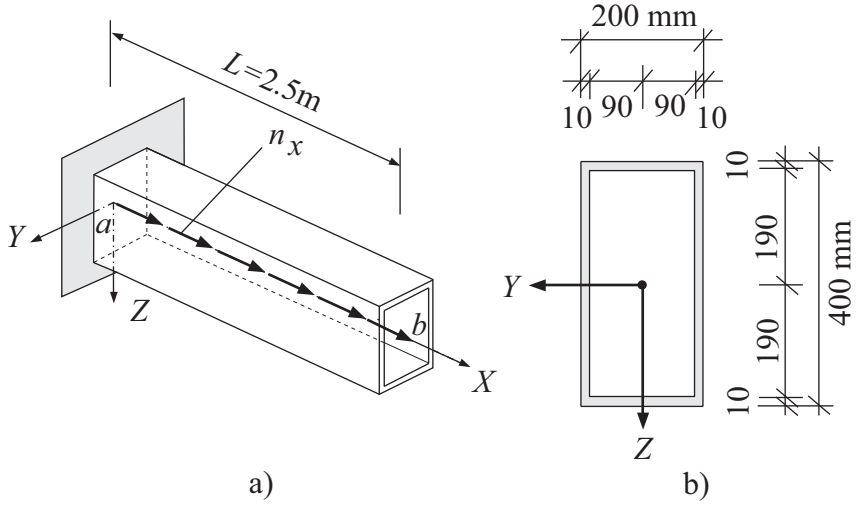

Figure 8: Cantilever beam with rectangular hollow cross-section: a) system, axial load, b) cross-section.

Cross-sectional parameters [29]		
Cross-sectional area	$A = 116 \cdot 10^{-4}$	m²
Shear area in the *y* - direction	$A_y = 25.26 \cdot 10^{-4}$	m²
Shear area in the *z* - direction	$A_z = 71.59 \cdot 10^{-4}$	m²
Second moment of area about the *y*-axis	$I_y = 24358 \cdot 10^{-8}$	m⁴
Second moment of area about the *z*-axis	$I_z = 8198 \cdot 10^{-8}$	m⁴
Polar moment of area	$I_p = I_y + I_z = 32557 \cdot 10^{-8}$	m⁴
Radius of gyration	$i_p = 16.75 \cdot 10^{-2}$	m
Torsion constant	$I_T = 18933.8 \cdot 10^{-8}$	m⁴
Secondary torsion constant	$I_{Ts} = 1953.6 \cdot 10^{-8}$	m⁴
Warping constant	$I_\omega = 157782 \cdot 10^{-12}$	m⁶
Warping-ordinate at the corner points	$\lvert\omega_R\rvert = 63.879 \cdot 10^{-2}$	m²

Table 4: Cross-sectional parameters [29].

Following torsional modal analyses have been performed by:

- proposed method (PM) - with only one finite element (FE)
- SOLID186 [3] -13920 FE
- BEAM188 [3] (warping restrained - WR) - number of 100 FE
- BEAM188 [3] (warping unrestrained - WU) - number of 100 FE

As show the analyses results in Table 5, the varying axial force has not influenced the eigefrequencies significantly. In opposite to open cross-section, the radius of gyration is much smaller for the rectangular hollow cross section (see Table 4), so by the axial force, the second order torsional stiffness GI_T^* is influenced negligible comparing to the Saint-Venant torsion stiffness GI_T. By larger axial force the buckling stability can be violated or the maximal strength limit can be exceeded in the considered case. It is also shown in Table 5 that the eigenfrequencies obtained by the standard beam finite elements (including also our new beam finite element) differ significantly from the ones obtained by the 3D solid finite elements (which is assumed as a benchmark solution). This fact relates with distortion of the closed thin-walled cross-section.

n_x [kNm^{-1}]	f_j [Hz]	PM	SOLID186	BEAM188 WR	BEAM188 WU
- 1 000	f_1	245.7	312.9	250.4	246.5
	f_2	738.5	837.4	754.2	739.9
	f_3	1234.3	1480.0	1265.4	1233.4
0	f_1	246.1	313.0	250.8	246.9
	f_2	739.3	837.8	754.9	740.6
	f_3	1235.7	1480.0	1266.6	1234.6
+1 000	f_1	246.5	313.3	251.1	247.2
	f_2	740.2	839.5	755.6	741.4
	f_3	1237.1	1481.0	1267.6	1235.8

Table 5: Eigenfrequencies of the cantilever beam with rectangular hollow cross-section.

4.3 Torsional modal analyses of a cantilever beam with rectangular hollow cross-section, subjected to a constant axial load.

A cantilever beam with rectangular hollow cross-section (Figure 9) is subjected to various constant axial force. The length of the beam is $L = 0.4$ m. The material properties and the cross-sectional parameters are listed in Table 1 and Table 6, respectively.

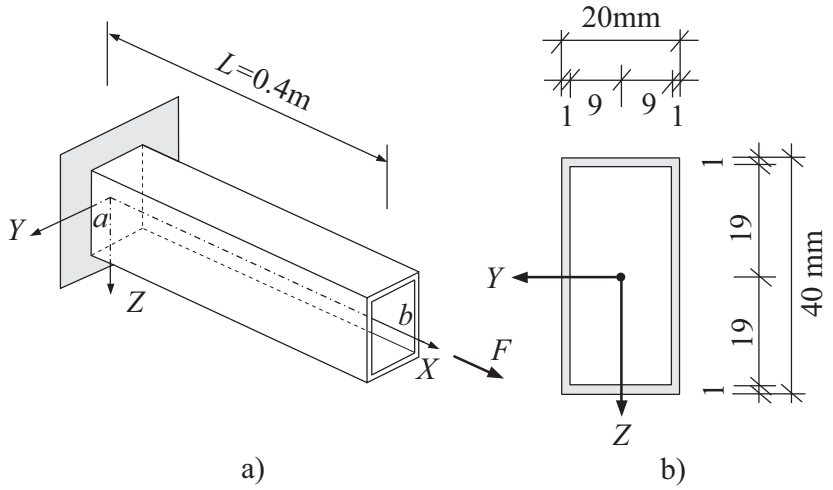

Figure 9: Cantilever beam with rectangular hollow cross-section:

Cross-sectional parameters [29]		
Cross-sectional area	$A = 0.116 \cdot 10^{-3}$	m²
Shear area in the *y* - direction	$A_y = 0.02526 \cdot 10^{-3}$	m²
Shear area in the *z* - direction	$A_z = 0.07159 \cdot 10^{-3}$	m²
Second moment of area about the *y*-axis	$I_y = 0.24358 \cdot 10^{-7}$	m⁴
Second moment of area about the *z*-axis	$I_z = 0.8198 \cdot 10^{-8}$	m⁴
Polar moment of area	$I_p = I_y + I_z = 0.32557 \cdot 10^{-7}$	m⁴
Radius of gyration	$i_p = 16.75 \cdot 10^{-3}$	m
Torsion constant	$I_T = 0.189338 \cdot 10^{-8}$	m⁴
Secondary torsion constant	$I_{Ts} = 0.19536 \cdot 10^{-8}$	m⁴
Warping constant	$I_\omega = 1.57782 \cdot 10^{-13}$	m⁶
Warping-ordinate at the corner points	$\lvert\omega_R\rvert = 63.879 \cdot 10^{-6}$	m²

Table 6: Cross-sectional parameters [29].

Similarly to the previous example, the torsional modal analyses have been performed. The constant axial force is denoted by N^{II}. Obtained results shown in Table 7 can be evaluated by the same way, as is done in the subchapter 4.2.

N^{II} [kN]	f_j [Hz]	PM	SOLID186	BEAM188 WR	BEAM18 WU
– 10	f_1	1544.6	2301.2	1556.5	1541.5
	f_2	4637.4	5492.4	4676.3	4624.8
	f_2	7740.2	-	7816.1	7709.3
0	f_1	1546.0	2303.9	1557.9	1542.9
	f_2	4641.58	5495.3	4980.5	4629.0
	f_3	7747.2	-	7823.0	7716.2
+ 10	f_1	1547.4	2305.8	1559.3	1544.3
	f_2	4645.8	5498.4	4684.6	4633.2
	f_3	7754.2	-	7829.9	7723.2
+ 20	f_1	1548.8	2307.3	1560.7	1545.6
	f_2	4650.0	5501.7	4688.8	4637.3
	f_3	7761.2	-	7836.8	7730.1
+ 30	f_1	1550.2	2308.5	1562.1	1547.0
	f_2	4654.2	5505.3	4692.9	4641.5
	f_3	7768.2	-	7843.7	7737.1
+ 40	f_1	1551.64	2309.7	1563.5	1548.4
	f_2	4658.43	5509.2	4697.1	4645.6
	f_3	7775.2	-	7850.5	7744.0

Table 7: Eigenfrequencies of the cantilever beam with rectangular hollow cross-section.

5 CONCLUSIONS

In this paper, the differential equation for the torsional deformation of a beam, subjected to variable axial forces, was formulated for Saint-Venant and non-uniform torsional deformations, including inertial line moments. The influence of the axial force on the torsional stiffness of the thin-walled beam was considered according to second-order torsional warping theory. For non-uniform torsion, the part of the bicurvature, caused by the bimoment, was taken into account as the warping degree of freedom, and the STMDE was also considered. A general semi-analytical solution of the differential equation was presented and the transfer matrix relation was established. Based on the relations of the transfer matrix method, a straight finite beam element with two nodes was derived. Omitting the external load, the relationship for the torsional free vibrations was obtained in the framework of the FEM. The numerical investigation involves torsional modal analysis of thin-walled beams with I cross-sections and rectangular hollow cross-sections. It was shown for I cross-section beam that the tensile axial forces result in a significant increase of the eigenfrequencies, whereas compressive axial forces lead to their decrease. On the other hand, the effect of axial force on the torsional eigenfrequencies is not significant by the rectangular hollow cross-sections beams. It was also shown by the rectangular hollow cross-sections that the eigenfrequencies obtained by the standard beam finite elements

as well by our new beam finite element differ significantly from the ones obtained by the SOLID186 finite element (which is assumed as a benchmark solution). This fact relates with distortion of the rectangular hollow thin-walled cross-sections. This is not considered in the beam finite elements used in our calculations.
The main novelties of the present contribution are:

- consideration of a variable axial force and of the STMDE in the differential equation for non-uniform torsion of thin-walled beams with open and closed cross-sections according to the theory of second-order torsional warping;
- formulation of the equations needed for the transfer matrix method and the FEM for elastostatic and modal analysis of non-uniformly twisted beams according to this theory;
- application of the presented new finite element equations for second order torsional warping modal analysis of thin-walled beams and comparison of the results with the ones computed with the help of commercial FEM codes.

REFERENCES

[1] M. Aminbaghai, J. Murin, J. Hrabovsky, H.A. Mang, Torsional warping eigenmodes including the effect of the secondary torsion-moment on the deformations*, Engineering Structures*, **106**, 299 – 316, 2016.

[2] I.C. Dikaros, E.J. Sapountzakis, A.K. Argyridi, Generalized warping effect in the dynamic analysis of beams of arbitrary cross section, *Journal of Sound and Vibration*, **369**, 119 – 146, 2016.

[3] ANSYS Swanson Analysis System, Inc., 201 Johnson Road, Houston, PA 15342/1300, USA.

[4] ADINA R & D, Inc. Theory and Modelling Guide. Volume I: ADINA. 2013.

[5] ABAQUS/CAE, Version 6.10-1, Dassault Systemes Simulia Corp. Providence, RI, USA.

[6] J.S. Przemieniecki, *Theory of matrix structural analysis*. McGraw-Hill Book Co., 1968.

[7] K.J. Bathe, A. Chaudhary, On the displacement formulation of torsion of shafts with rectangular cross-sections, *International Numerical Methods in Engineering*, **18**, 1565 – 1568, 1982.

[8] E.J. Sapountzakis, V.J. Tsipiras, A.K. Argyridi, Torsional vibration analysis of bars including secondary torsional shear deformation-effect by the boundary element method, *Journal of Sound and Vibration*, **355**, 208 – 231, 2015.

[9] E.J. Sapountzakis, V.G. Mokos, Dynamic analysis of 3-D beam elements including warping and shear deformation-effects, *Solids and Structures*, **43**, 6707 – 6726, 2016.

[10] E.J. Sapountzakis, V.J. Tsipiras, Nonlinear non-uniform torsional vibration, *Non-linear Mechanics*, **329**, 1853 – 1874, 2010.

[11] E.J. Sapountzakis, I.C. Dikaros, Non-linear flexural–torsional dynamic analysis of beams of arbitrary cross section by BEM, *Non-linear Mechanics*, **46**, 782 – 794, 2011.

[12] S.A. Sina, H. Haddadpour, H.M. Navazi, Nonlinear free vibration of thin-walled beams in torsion, *Acta Mechanica*, **233**, 2135 – 2151, 2012.

[13] S.J. Lee, S.B. Park, Vibrations of Timoshenko beams with isogeometric approach, *Applied Mathematical Modelling*, **37**, 9174 – 9190, 2013.

[14] S. Stoykov, P. Ribeiro, Non-linear vibrations of beams with non-symmetrical cross sections, *Non-linear Mechanics*, **55**, 153 – 169, 2013.

[15] S.A. Sina, H. Haddadpour, Axial–torsional vibrations of rotated pretwisted thin-walled composite beams, *Mechanical Sciences*, **80**, 93 – 101, 2014.

[16] K.F. Ferradi, X. Cespedes, A new beam element with transversal and warping eigenmodes, *Computers and Structures*, **131**, 12 – 33, 2014.

[17] K. Yoon, D.N. Kim, Geometrically nonlinear analysis of functionally graded 3D beams considering warping effects, *Composite Structures*, **132**, 1231 – 1247, 2015.

[18] J. Murin, M. Aminbaghai, V. Kutis, V. Kralovic, V. Goga, H.A. Mang, A new 3D Timoshenko finite beam element including non-uniform torsion of open and closed cross sections, *Engineering Structures*, **59**, 153-60, 2014.

[19] J. Murin, V. Goga, M. Aminbaghai, J. Hrabovsky, T. Sedlar, V. Kutis, J. Paulech, Warping free vibration of thin-walled beams: Experimental verification and Modelling, J. Kruis, Y. Tsompanakis and B.H.V Topping eds. *Proceedings of the 15th International Conference on Civil, Structural and Environmental Engineering Computing*., Civil-Comp Press, Stirlingshire, Scotland, Prague, 2015, pp. 12.

[20] M. Arici, M.F. Granata, Unified theory for analysis of curved thin-walled girders with open and closed cross section through HSA method, *Engineering Structures*, **113**, 299-314, 2016.

[21] J. Freund, A. Karakoc, Warping displacement of Timoshenko beam model, *Solid and Structures*, **92-93**, 9-16, 2016.

[22] S. Stoykov, E. Manoach, S. Margenov, An efficient 3D numerical beam model based on cross-sectional analysis and Ritz approximations, *ZAMM*, **96**, 791-812, 2016.

[23] J. Xiaoliang, G.K. Narahara, Prediction of coupled torsional-axial vibrations of drilling tool with boundary conditions, *Manufacturing Science and Technology*, **13**, 24-36, 2016.

[24] T. Mondal, S. Prakash, Nonlinear finite-element analysis of RC bridge columns under torsion with and without axial compression, *Bridge Engineering*, **21**, 2016 doi: 10.1061/(ASCE)BE.1943-5592.0000798.

[25] J. Fink, Besondere Stabilitätsprobleme im Stahlbau [*in German; Specific stability issues in steel construction*], Lecture Manuscript, Technical University of Vienna, 2005.

[26] H. Rubin, Wölbkrafttorsion von Durchlaufträgern mit konstantem Querschnitt unter Berücksichtigung sekundärer Schubverformung [in German; Torsional warping theory including the secondary torsion-moment deformation-effect for beams with constant cross-section], Stahlbau **74**, 826-842, 2005.

[27] H. Rubin, Lösung linearer Differentialgleichungen beliebiger Ordnung mit Polynomkoeffizienten und Anwendung auf ein baustatisches Problem [in German; Solution concept for linear differential equations with nonlinear polynomial coefficients and application to engineering problems], *Zeitschrift für Angewandte Mathematik und Mechanik*, **76**-2, 105–117, 1996.

[28] Wolfram Mathematica 9.0.1.0, Wolfram Research 2013.

[29] DUENQ, Version 7.01, Dlubal.

[30] RSTAB 8.06, Ingenieur - Software Dlubal GmbH, Tiefenbach 2006.

[31] M. Schneider-Bürger, *Stahlbau-Profile*, Verlag Stahleisen GmbH, Düsseldorf 2001, volume 23.

[32] H. Rubin, Baustatik 2 [*in German; Structural analysis 2*]. Lecture Manuscript, Technical University of Vienna, 2005.

[33] RFEM 5.07, Ingenieur - Software Dlubal GmbH, Tiefenbach 2006.

[34] M. Aminbaghai, J. Murin, G. Balduzzi, J. Hrabovsky, G. Hochreiner, H. A. Mang, Second-order torsional warping theory considering the secondary torsion-moment deformation effect. (Sent for publication in Int. Journal of Engineering Structures), 2017.